



OPEN ACCESS

EDITED BY

Rocco Trisolini,
Agostino Gemelli University Polyclinic
(IRCCS), Italy

REVIEWED BY

Fiori Alite,
Geisinger Commonwealth School of
Medicine, United States
Franca Chierichetti,
Azienda Provinciale per i Servizi
Sanitari (APSS), Italy

*CORRESPONDENCE

Ying Liang
liangy_2000@sina.com
Tao Sun
tao.sun@siat.ac.cn

[†]These authors have contributed
equally to this work

SPECIALTY SECTION

This article was submitted to
Cancer Imaging and
Image-directed Interventions,
a section of the journal
Frontiers in Oncology

RECEIVED 28 July 2022

ACCEPTED 25 October 2022

PUBLISHED 10 November 2022

CITATION

Wumener X, Zhang Y, Wang Z,
Zhang M, Zang Z, Huang B, Liu M,
Huang S, Huang Y, Wang P, Liang Y
and Sun T (2022) Dynamic FDG-PET
imaging for differentiating metastatic
from non-metastatic lymph nodes of
lung cancer.

Front. Oncol. 12:1005924.

doi: 10.3389/fonc.2022.1005924

COPYRIGHT

© 2022 Wumener, Zhang, Wang, Zhang,
Zang, Huang, Liu, Huang, Wang,
Liang and Sun. This is an open-access
article distributed under the terms of
the [Creative Commons Attribution
License \(CC BY\)](https://creativecommons.org/licenses/by/4.0/). The use, distribution
or reproduction in other forums is
permitted, provided the original
author(s) and the copyright owner(s)
are credited and that the original
publication in this journal is cited, in
accordance with accepted academic
practice. No use, distribution or
reproduction is permitted which does
not comply with these terms.

Dynamic FDG-PET imaging for differentiating metastatic from non-metastatic lymph nodes of lung cancer

Xieraili Wumener¹, Yarong Zhang¹, Zhenguo Wang²,
Maoqun Zhang¹, Zihan Zang³, Bin Huang¹, Ming Liu¹,
Shengyun Huang¹, Yong Huang¹, Peng Wang¹,
Ying Liang^{1*†} and Tao Sun^{2*†}

¹Department of Nuclear Medicine, National Cancer Center, National Clinical Research Center for Cancer, Cancer Hospital & Shenzhen Hospital, Chinese Academy of Medical Sciences and Peking Union Medical College, Shenzhen, China, ²Paul C. Lauterbur Research Center for Biomedical Imaging, Shenzhen Institute of Advanced Technology, Chinese Academy of Sciences, Shenzhen, China, ³Shenzhen Middle School, Shenzhen, China

Objectives: ¹⁸F-fluorodeoxyglucose (FDG) PET/CT has been widely used in tumor diagnosis, staging, and response evaluation. To determine an optimal therapeutic strategy for lung cancer patients, accurate staging is essential. Semi-quantitative standardized uptake value (SUV) is known to be affected by multiple factors and may fail to differentiate between benign and malignant lesions. Lymph nodes (LNs) in the mediastinal and pulmonary hilar regions with high FDG uptake due to granulomatous lesions such as tuberculosis, which has a high prevalence in China, pose a diagnostic challenge. This study aims to evaluate the diagnostic value of the quantitative metabolic parameters derived from dynamic ¹⁸F-FDG PET/CT in differentiating metastatic and non-metastatic LNs in lung cancer.

Methods: One hundred and eight patients with pulmonary nodules were enrolled to perform ¹⁸F-FDG PET/CT dynamic + static imaging with informed consent. One hundred and thirty-five LNs in 29 lung cancer patients were confirmed by pathology. Static image analysis parameters including LN-SUVmax, LN-SUVmax/primary tumor SUVmax (LN-SUVmax/PT-SUVmax), mediastinal blood pool SUVmax (MBP-SUVmax), LN-SUVmax/MBP-SUVmax, and LN-SUVmax/short diameter. Quantitative parameters including K_1 , k_2 , k_3 and K_i and of each LN were obtained by applying the irreversible two-tissue compartment model using in-house Matlab software. K_i/K_1 was computed subsequently as a separate marker. We further divided the LNs into mediastinal LNs ($N=82$) and pulmonary hilar LNs ($N=53$). Wilcoxon rank-sum test or Independent-samples T-test and receiver-operating characteristic (ROC) analysis was performed on each parameter to compare the diagnostic efficacy in differentiating lymph node metastases from inflammatory uptake. $P<0.05$ were considered statistically significant.

Results: Among the 135 FDG-avid LNs confirmed by pathology, 49 LNs were non-metastatic, and 86 LNs were metastatic. LN-SUVmax, MBP-SUVmax, LN-SUVmax/MBP-SUVmax, and LN-SUVmax/short diameter couldn't well differentiate metastatic from non-metastatic LNs ($P>0.05$). However, LN-SUVmax/PT-SUVmax have good performance in the differential diagnosis of non-metastatic and metastatic LNs ($P=0.039$). Dynamic metabolic parameters in addition to k_3 , the parameters including K_1 , k_2 , K_i , and K_i/K_1 , on the other hand, have good performance in the differential diagnosis of metastatic and non-metastatic LNs ($P=0.045$, $P=0.001$, $P=0.001$, $P=0.001$, respectively). For ROC analysis, the metabolic parameters K_i (AUC of 0.672 [0.579-0.765], sensitivity 0.395, specificity 0.918) and K_i/K_1 (AUC of 0.673 [0.580-0.767], sensitivity 0.570, specificity 0.776) have good performance in the differential diagnosis of metastatic from non-metastatic LNs than SUVmax (AUC of 0.596 [0.498-0.696], sensitivity 0.826, specificity 0.388), included the mediastinal region and pulmonary hilar region.

Conclusion: Compared with SUVmax, quantitative parameters such as K_1 , k_2 , K_i and K_i/K_1 showed promising results for differentiation of metastatic and non-metastatic LNs with high uptake. The K_i and K_i/K_1 had a high differential diagnostic value both in the mediastinal region and pulmonary hilar region.

KEYWORDS

dynamic imaging, PET/CT, ^{18}F -FDG, lung cancer, lymph Node

Introduction

Lung cancer is the leading cause of cancer-related deaths worldwide. In China, it ranks first with a 30% mortality rate (1, 2). Accurate staging of lymph nodes (LNs) is an important prognostic factor and is critical for treatment planning of lung cancer (3). Because the 5-year survival for stage IA lung cancer patients reaches 92%, while the IVA stage drops to 10% (4). For N-staging, the 5-year survival for stage N0 reaches 56%, while the N3 stage drops to 6% (5). Therefore, early diagnosis and accurate stage play an important role in improving survival rates.

^{18}F -fluorodeoxyglucose (FDG) positron emission tomography/CT (PET/CT) has been widely used in tumor diagnosis, staging, and response evaluation. The National Comprehensive Cancer Network (NCCN) recommends ^{18}F -FDG PET/CT for clinical staging (6). However, ^{18}F -FDG PET/CT has limited sensitivity and specificity for detecting metastatic mediastinal LNs of non-small cell lung cancer (NSCLC) (7, 8). Preceding Meta-analysis (9) concluded that the sensitivity of ^{18}F -FDG PET/CT for mediastinal staging in NSCLC patients was 0.81(0.70-0.89) and the specificity was 0.79(0.70-0.87), but the contribution of endemic infectious disease areas remains to be discussed. Because, several benign FDG-avid LNs exist in granulomatous disease, tuberculosis, interstitial lung disease,

and other infectious conditions including pneumonia (10, 11). Stephen et al. (12) concluded that, compared to non-endemic regions with endemic infectious disease, ^{18}F -FDG PET/CT has a 16% lower average specificity in endemic regions (77% [73%-80%] vs. 61% [49%-72%]). In addition to that, the standard uptake value(SUV) as a semi-quantitative metabolic parameter is affected by multiple factors, such as scan time, blood glucose level, etc ... Therefore, SUV measurement of FDG activity is sometimes challenging to discriminate between benign and malignant in regions with a high prevalence of tuberculosis and granulomatous lesions, such as China. Thus, reliable imaging biomarkers for N-staging in lung cancer are crucial.

Radiopharmaceutical distribution is a dynamic process that varies widely in diseases and individuals (13). Dynamic PET/CT (dPET/CT) continuously acquires imaging data over a certain time period. Based on proper kinetic modeling, absolute quantitative metabolic parameters can be obtained, e.g., net influx rate K_i , tumor blood flow K_1 , phosphorylation rate k_3 , etc. (14). Compared to static PET/CT (acquired about 60 min after FDG injection), dPET/CT extracts physiological and biochemical parameters and better reveals the pathophysiological mechanisms of diseases. These parameters were proven to be able to differentiate between benign and malignant (14). Previous studies have confirmed the advantages

of dPET/CT in the diagnosis of lung cancer and inflammatory lung lesions (15–19), but reports regarding FDG-avid LNs in lung cancer were seldom seen.

In the present study, we compared ^{18}F -FDG PET/CT dynamic imaging with static imaging and investigated the value of their metabolic parameters in the differential diagnosis between metastatic and non-metastatic FDG-avid LNs, especially in the mediastinal and hilar regions.

Materials and methods

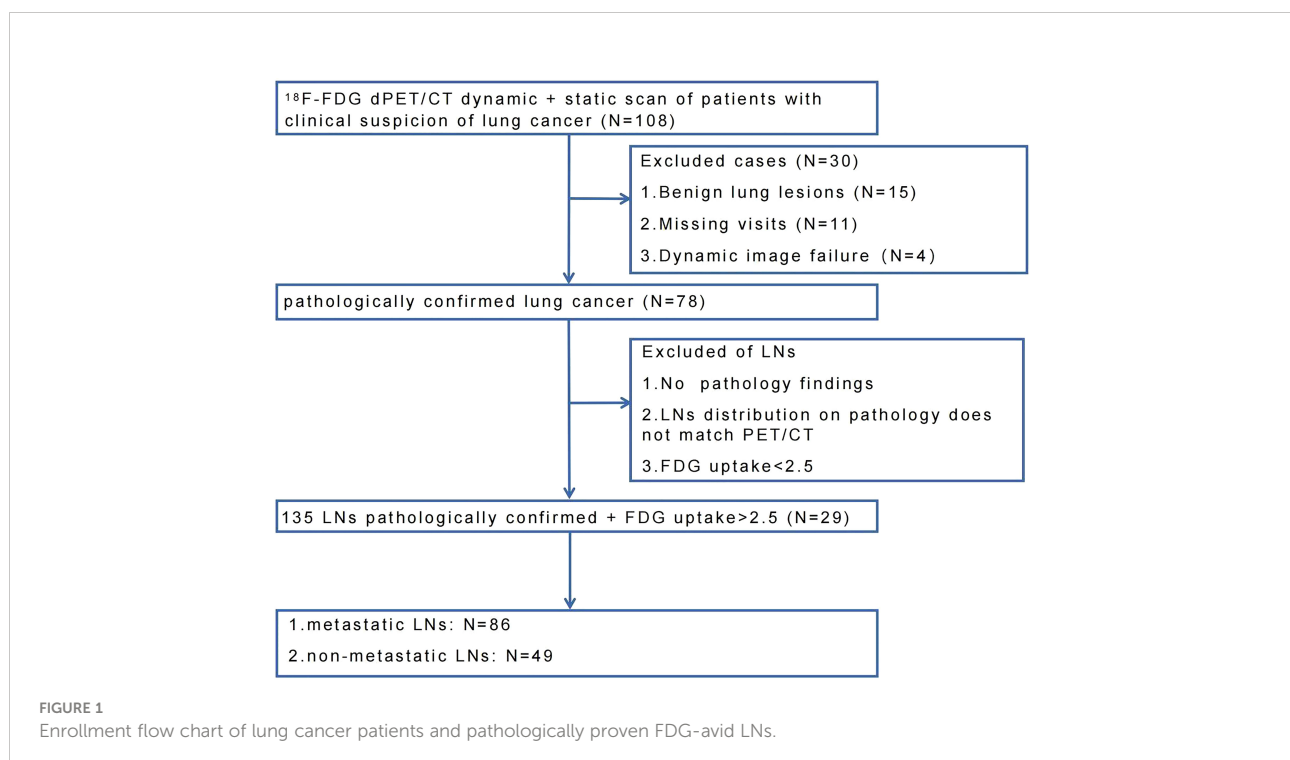
Patients

This study was approved by the ethics committee of Cancer Hospital & Shenzhen Hospital, Chinese Academy of Medical Sciences (KYLH2022-1). A total of 108 patients were enrolled in this study from May 2021 to March 2022. All patients underwent chest CT and PET/CT scans for clinical suspicion of lung cancer without treatment. All patients signed a written informed consent before the PET/CT imaging. Four patients failed to finish dPET/CT scans due to physiological factors (e.g., failure to hold urine, nervous). Eleven patients were lost to follow-up. Ninety-three patients underwent puncture and/or surgery within two weeks after dPET/CT scan. Fifteen patients had benign pathological results, and seventy-eight patients were pathologically confirmed to have lung cancer. In these 78 lung

cancer patients, LNs were excluded following the criteria: 1) SUVmax less than 2.5; 2) mismatch of distribution between PET/CT scan and puncture/surgery; 3) no proven pathology. Finally, 135 FDG-avid (SUVmax >2.5) LNs of 29 lung cancer patients were included and remarked, of which 86 LNs were confirmed metastatic and 49 LNs were confirmed non-metastatic. The flow chart of LNs enrollment was shown in Figure 1.

PET/CT data acquisition and reconstruction

All patients fasted for at least 6 hours before the PET/CT scan (Discovery MI PET/CT, GE Healthcare, Milwaukee, USA). Blood glucose was maintained at lower than 8.0 mmol/L. The patients first underwent a whole-body CT scan from the head to the mid-femur in a supine position with the arms raised. The CT parameters were tube voltage of 120 kV, tube current setting of 10–220 mA, pitch of 1.375:1 and noise index of 20. The chest region PET scans were initiated immediately after the injection of ^{18}F -FDG (264.8 ± 37 MBq) from an intravenous indwelling needle. The total dynamic scans lasted for 65 minutes. Dynamic scan data were partitioned into 28 frames as follows: 6×10 s, 4×30 s, 4×60 s, 4×120 s, 10×300 s. An additional whole-body static PET scan was performed at the end of the dynamic acquisition. The attenuation correction was performed using



CT data, and reconstruction was performed using the Block sequential regularized expectation maximization reconstruction algorithm (BSREM) with 25 iterations and 2 subsets.

PET/CT data analysis

Dynamic parameters of K_1 , k_2 , k_3 and K_i were obtained based on the two-tissue irreversible compartment model. The image-derived input function (IDIF) was extracted from the ascending aorta by drawing a 10-mm-diameter ROI on six consecutive slices in an image obtained by combining early time frames (0–60 s), where the effects of motion and partial volume were less prominent than in the left ventricle. The uptake difference in blood and plasma was not accounted for in this study. In this model, we assumed unidirectional uptake of ^{18}F -FDG (i.e., $k_4 = 0$), with irreversible trapping in tissue as ^{18}F -FDG-6-PO₄ (20). Parametric images of each dynamic scan were generated using Voxel-based analysis. Given a large number of voxels in a whole-body image, the Lawson-Hanson non-negative least squares algorithm was applied to solve a linearized problem instead of the conventional nonlinear one (21). The 3D volume-of-interest (VOI) of each lesion was delineated using the semi-automatic methods with a threshold of 40% SUVmax in ITK-snap software (version 4.9). For the lesions with surrounding physiological uptake, 3D VOI was manually delineated slice-by-slice by two experienced nuclear medicine physicians. Then the segmented VOI was applied to the K_1 , k_2 , k_3 and K_i parametric images to extract the quantitative measurements of each scan.

Static images were independently reviewed by two nuclear medicine physicians with more than 10 years of experience. LNs location was classified according to the International Association for the Study of Lung cancer (IASLC) lymph node map (22) and divided into the mediastinal region (zone 1 to 9) and pulmonary hilar region (zone 10 to 12). N-stage is based on the 8th edition of the TNM classification of lung cancer (23). LN-SUVmax and primary tumor (PT-SUVmax) were measured at the maximum cross-sectional level of the LNs and primary tumor. Mediastinal blood pool SUVmax (MBP-SUVmax) was measured by placing an ROI within the lumen of the aortic arch. The long diameter, short diameter, and CT density of the LNs were measured on a 5-mm CT image in the same axial direction as the SUVmax of LNs were measured.

Numerous previous studies have explored the threshold for LN positivity, including a SUVmax cut-off of 2.5 (24–28). The main purpose of this study was to further investigate the value of dPET/CT imaging for the differential diagnosis of high FDG uptake LNs. Therefore, in the context of previous studies of nodes and the stability and accuracy of the dynamic processing software, we considered SUVmax > 2.5 (axial images) as FDG-avid LNs. In case of disagreement between the two raters, the consensus was reached by discussion.

Pathological evaluation

Two independent pathologists (over ten years of experience in lung cancer pathology) evaluated samples of dissected tissue. All dissected tumors and lymph nodes were sectioned and examined conventionally using hematoxylin-eosin staining. Immunohistochemical staining was also performed at the pathologist's discretion.

Statistical analysis

As the data distribution was non-normal, quantitative metrics of LNs were compared between groups using Wilcoxon rank-sum test or Independent-samples T-test. The receiver-operating characteristic (ROC) analysis was performed on each parameter to reveal the diagnostic efficacy in differentiating nonmetastatic and metastatic LNs with high FDG uptake. The difference in the area under curve (AUC) was determined by Delong's test. A *P*-value less than 0.05 were considered statistically significant. All statistical analyses were performed in R statistical software (version 4.1.1).

Results

Characteristics of the patients and LNs

Patient and LNs characteristics were presented in Table 1. Among the 29 patients who underwent dPET/CT imaging, the average age was 62.0 (62.0 ± 10.20) years, and the number of male and female patients was 17 (58.60%) and 12 (41.40%), respectively. The pathological types of the primary tumor were adenocarcinoma in 17 patients (58.60%), squamous cell carcinoma in 9 patients (32.14%), small cell carcinoma in 2 patients (6.90%) and atypical carcinoid tumor in 1 patient (3.45%).

Among the 135 LNs pathologically confirmed, 49 were non-metastatic (49/37.12%) and 86 were metastatic including 60 (44.44%) adenocarcinoma, 14 (10.61%) squamous cell carcinoma, and 12 (9.09%) small cell carcinoma. The LNs were divided into the mediastinal region (82/60.74%) and the pulmonary hilar region (53/39.26%) according to their distribution.

PET/CT parameter analysis of FDG-avid LNs

Table 2 showed the parameter analysis of FDG-avid LNs in both dPET/CT and static PET/CT. In static PET/CT, LN-SUVmax/PT-SUVmax was statistically significant to

TABLE 1 Characteristics of the patients and LNs.

Characteristic	Distribution
Sex Male	17 (58.60%)
Age (years) Mean \pm SD	62.0 \pm 10.20
Lobar distribution of the primary tumor(N)	29
RUL/RML/RLL	4 (13.80%)/5 (17.20%)/3 (10.30%)
LUL/LLL	9 (31.0%)/8 (27.60%)
Histopathological type of the primary tumor (N)	29
Adenocarcinoma	17 (58.60%)
Squamous cell carcinoma	9 (32.14%)
Small cell carcinoma	2 (6.90%)
Atypical carcinoid tumor	1 (3.45%)
Histopathological type of the LNs (N)	135
Non-metastatic group(N)	49
Cancer-free	49 (37.12%)
Metastatic group(N)	86
Adenocarcinoma	60 (44.44%)
Squamous cell carcinoma	14 (10.61%)
Small cell carcinoma	12 (9.09%)
LN's distribution(N)	135
mediastinal LNs	82 (60.74%)
pulmonary hilar LNs	53 (39.26%)

SD standard deviation, RUL right upper lobe, RML right middle lobe, RLL right lower lobe, LUL left upper lobe, LLL left lower lobe.

differentiate non-metastatic and metastatic LNs (0.600 [\pm 0.304] vs 0.730 [\pm 0.411], $P=0.039$, Figure 2G). The CT density, length diameter, short diameter, as well as LN-SUVmax (Figure 2F), MBP-SUVmax, LN-SUVmax/short diameter (Figure 2I), and

LN-SUVmax/MBP-SUVmax (Figure 2H) in static PET/CT, could not well differentiate metastatic and non-metastatic LNs ($P>0.05$) Table 3.

In dPET/CT, K_i and K_i/K_1 in non-metastatic group (0.016 ml/g/min and 0.056) were lower than those in metastatic group (0.019 ml/g/min and 0.104), and the differences were statistically significant ($P=0.001$, $P=0.001$, respectively, Figures 2D, E). K_1 and k_2 in non-metastatic group (0.253 ml/g/min and 0.666 min⁻¹) were higher than those in metastatic group (0.205 ml/g/min and 0.350 min⁻¹) with statistical significance ($P=0.045$, $P=0.001$, respectively, Figure 2A, B). However, the k_3 did not show significant difference between groups (0.039 and 0.044 min⁻¹, $P>0.05$, Figure 2C).

The ROC curves and cut-off values for PET/CT metabolic parameters

By ROC curve analysis, the LN-SUVmax/PT-SUVmax cut-off value of 0.236, AUC of 0.566 (0.462-0.670), sensitivity of 0.999 and specificity of 0.204, respectively.

In ROC curve analysis (Figure 3A), the cut-off value of K_1 , k_2 , K_i and K_i/K_1 were 0.234 (AUC of 0.604, sensitivity 0.581, specificity 0.612), 0.549 (AUC of 0.677, sensitivity 0.767, specificity 0.571), 0.022 (AUC of 0.672, sensitivity 0.395, specificity 0.918) and 0.093 (AUC of 0.673, sensitivity 0.570, specificity 0.776), respectively.

Delong's test did not reveal any significant differences between SUVmax and other dynamic parameters including K_1 , k_2 , k_3 , K_i , and K_i/K_1 ($P>0.05$). However, we performed Delong's test with LN-SUVmax/P-SUVmax and found that the metabolic parameter K_i was statistically different ($P=0.26$).

TABLE 2 FDG-avid LNs PET/CT characteristics and parameters analysis.

Characteristic	Non-metastatic group (N=49)	Metastatic group (N=86)	P Value
Density (HU)	43.00 [34.00;57.00]	38.00 [30.00;49.00]	0.147
Length diameter (cm)	1.10 [1.00;1.40]	1.10 [1.00;1.50]	0.292
Short diameter (cm)	0.80 [0.70;1.00]	1.00 [0.80;1.10]	0.057
LN-SUVmax	5.10 [3.70;6.50]	5.70 [4.43;8.23]	0.062
MBP-SUVmax	2.00 [1.70;2.00]	1.90 [1.70;2.20]	0.293
LN-SUVmax/PT-SUVmax	0.600 (\pm 0.304) [▲]	0.730 (\pm 0.411) [▲]	0.039*
LN-SUVmax/MBP-SUVmax	2.900 [1.900;3.529]	3.114 [2.402;4.608]	0.087
LN-SUVmax/Short diameter	6.167 [3.643;8.286]	6.854 [4.925;9.150]	0.256
K_1 (ml/g/min)	0.253 [0.145;0.405]	0.205 [0.123;0.318]	0.045*
k_2 (min ⁻¹)	0.666 [0.359;0.882]	0.350 [0.187;0.533]	0.001*
k_3 (min ⁻¹)	0.039 [0.027;0.059]	0.044 [0.028;0.064]	0.481
K_i (ml/g/min)	0.016 [0.009;0.020]	0.019 [0.013;0.028]	0.001*
K_i/K_1	0.056 [0.024;0.085]	0.104 [0.048;0.250]	0.001*

[▲]LN-SUVmax/PT-SUVmax values was expressed as mean \pm standard deviation (Independent-samples T-test), and the remaining indicators were expressed as median (interquartile spacing, Wilcoxon rank-sum test).

*stands for statistically significant difference.

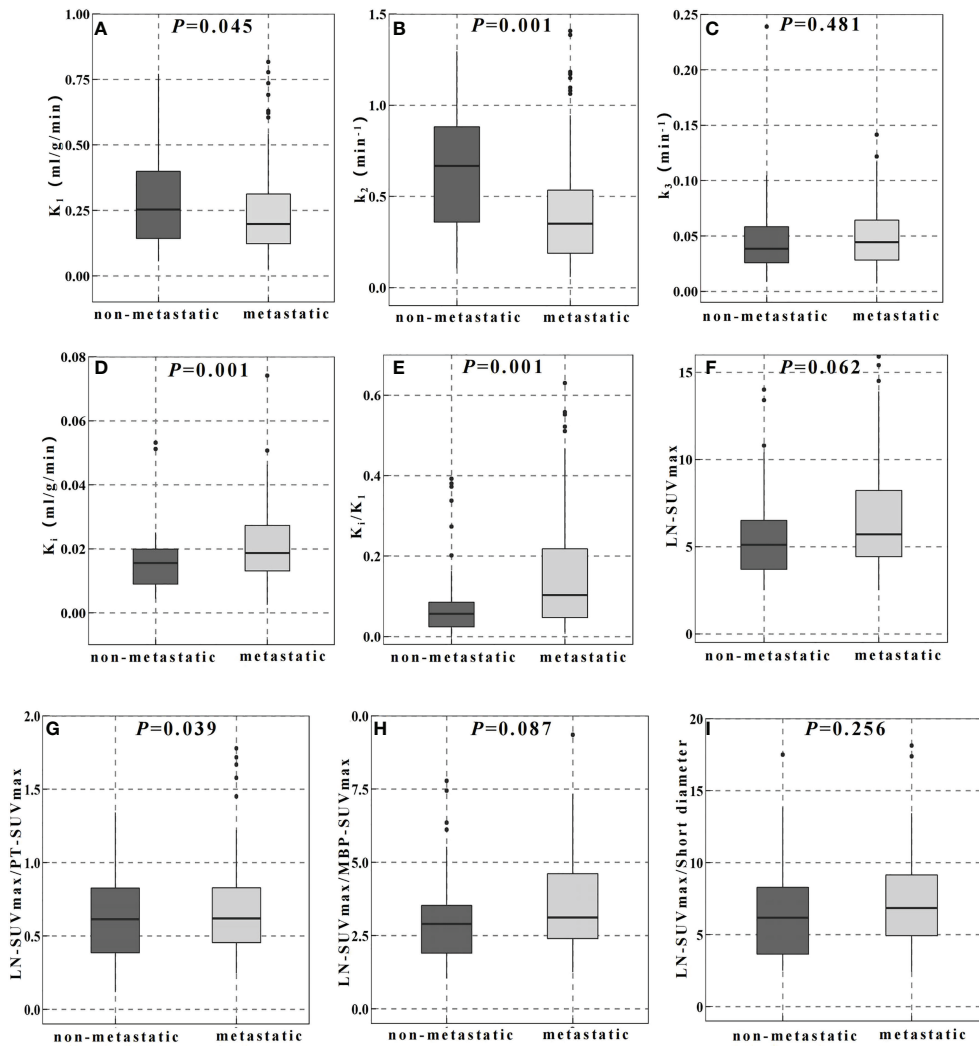


FIGURE 2 Comparison of dynamic (A–E) and static (F–I) PET/CT metabolic parameters in the differential diagnosis of FDG-avid LNs.

TABLE 3 Diagnostic efficacy of PET/CT metabolic parameters.

Characteristic	Sensitivity	Specificity	cut-off value	AUC[95% CI]	P Value */P Value ▲
SUVmax	0.826	0.388	4.050	0.596 [0.498-0.696]	–
LN-SUVmax/PT-SUVmax	0.999	0.204	0.236	0.566 (0.462-0.670)	–
K ₁ (ml/g/min)	0.581	0.612	0.234	0.604 [0.582-0.772]	0.910/0.602
K ₂ (min ⁻¹)	0.767	0.571	0.549	0.677 [0.584-0.774]	0.144/0.088
K _i (ml/g/min)	0.395	0.918	0.022	0.672 [0.579-0.765]	0.059/0.026
K _i /K ₁	0.570	0.776	0.093	0.673 [0.580-0.767]	0.115/0.838

*Delong's test comparison with SUVmax. ▲Delong's test comparison with LN-SUVmax/PT-SUVmax.

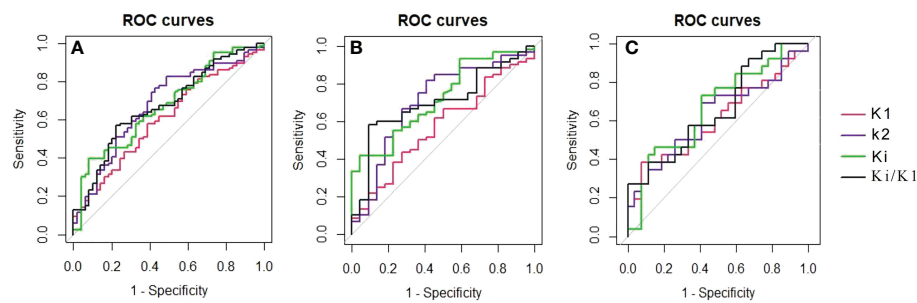


FIGURE 3

The ROC curves showed each metabolic parameter for the differential diagnosis of non-metastatic and metastatic FDG-avid LNs in all lesions (A), the mediastinal region (B) and the pulmonary hilar region (C).

FDG-avid LNs analysis between the mediastinal region and pulmonary hilar region

According to the results of the second part of the statistics, LN-SUVmax/PT-SUVmax, K_1 , K_2 , K_i , and K_i/K_1 were selected for further study. By ROC curve analysis in Figure 2, 3 in mediastinal region, the cut-off value of LN-SUVmax/PT-SUVmax, K_1 , k_2 , K_i and K_i/K_1 were 0.437 (AUC of 0.614 [0.453-0.775], sensitivity 0.833, specificity 0.500), 0.250 (AUC of 0.571, sensitivity 0.667, specificity 0.500), 0.526 (AUC of 0.705, sensitivity 0.817, specificity 0.591), 0.022 (AUC of 0.721, sensitivity 0.417, specificity 0.955) and 0.093 (AUC of 0.702, sensitivity 0.583, specificity 0.909), respectively. In pulmonary hilar region, the cut-off value of LN-SUVmax/PT-SUVmax, K_1 , k_2 , K_i and K_i/K_1 were 0.720 (AUC of 0.589 [0.431-0.747], sensitivity 0.577, specificity 0.677), 0.096 (AUC of 0.613, sensitivity 0.385, specificity 0.926), 0.662 (AUC of 0.623, sensitivity 0.692, specificity 0.593), 0.017 (AUC of 0.667, sensitivity 0.731, specificity 0.593) and 0.231 (AUC of 0.660, sensitivity 0.385, specificity 0.889), respectively.

The metabolic parameter K_i and K_i/K_1 have better diagnostic performance than other parameters both in the mediastinal region and pulmonary hilar region.

Discussion

Clinical concerns have been raised for differential diagnosis of metastatic and non-metastatic LNs in N-staging of lung cancer to reduce the false-positive rate. In this study, we found the dPET/CT quantitative metabolic parameters K_1 , k_2 , K_i and K_i/K_1 had higher diagnostic efficacy than SUVmax.

The quantification of FDG uptake using SUVmax is the most used PET-derived parameter used as a biomarker of glucose metabolism for both diagnostic and follow-up purposes. However, metabolic parameters of dynamic PET/CT, such as K_i (the net influx rate), K_1 (the surrogate of perfusion), k_2 (the

extraction) and k_3 (the phosphorylated rate) recently emerged for diagnosis, differential diagnosis, and efficacy evaluation (29–32). Zhen et al. (33) concluded that, in a study of subcutaneous and *in situ* models of NSCLC in a mouse model, the dynamic metabolic parameter K_i could effectively differentiate between inflammation and tumor and could offer an assessment for inflammations at different locations of the body. Qing et al. (34) revealed that the dynamic metabolic parameter K_i had a higher AUC value than SUVmax in the differential diagnosis of benign and malignant pulmonary nodules, and that K_i could better distinguish benign from malignant nodules. These metabolic parameters more accurately represent the different stages of FDG metabolism and thus reflect the pathophysiological mechanisms of the disease. However, these previous studies have focused on primary tumors, and very few have been used to identify benign and malignant LNs.

Yang et al. (35) found in their lung cancer study, K_i value in the primary group of metastatic was higher than that of non-metastatic ($0.050 \pm 0.005 \text{ min}^{-1}$ vs. $0.026 \pm 0.004 \text{ min}^{-1}$, $P < 0.001$), and K_i value of metastatic LN in group metastatic was higher than that in group primary tumor ($0.033 \pm 0.005 \text{ min}^{-1}$ vs. $0.016 \pm 0.003 \text{ min}^{-1}$, $P < 0.01$). Kornelia Kajary et al. (36) found in their breast cancer study, the K_i values were higher in the positive LNs group than in the negative LNs group (0.039 vs. 0.023, $P = 0.0315$), but K_1 , k_2 , k_3 were not statistically different in the differential diagnosis of non-metastatic and metastatic LNs. In our study, compared to SUVmax, the dynamic metabolic parameters K_1 , k_2 , K_i and K_i/K_1 had higher differential diagnostic efficacy of metastatic and non-metastatic FDG-avid LNs in lung cancer. The K_i and K_i/K_1 values in the non-metastatic group were lower than those in the metastatic group. But the K_1 and k_2 values in the non-metastatic group were higher than those in the metastatic group. By ROC curve analysis, SUVmax had high sensitivity (0.826) but low specificity (0.388) in differentiating metastatic from non-metastatic FDG-avid LNs. On the contrary, K_i had high specificity (0.918), but low sensitivity (0.395). As a result, K_i seemed to be a good compensation for SUVmax. We considered

the main reason for the low sensitivity of K_i is that we focused on LNs with FDG uptake > 2.5 and excluded the LNs with low uptake. In addition to that, among the 37 (37/49) non-metastatic FDG-avid LNs, the pathological type of the primary focus was adenocarcinoma. Whether dynamic metabolic parameters differ between pathological types requires further study.

To further improve the diagnostic efficacy of SUVmax, James Cerfolio first proposed the use of LN-SUVmax/PT-SUVmax to identify benign and malignant mediastinal LNs in lung cancer (37). Subsequently, Serra Fortuny et al. concluded that LN-SUVmax/PT-SUVmax is a good predictor of lymph node metastasis in NSCLC and the accuracy of mediastinal malignant LNs increased to 70% when using a 0.4 cut-off (38). Yang et al. (27) concluded that, when the LN-SUVmax/PT-SUVmax cut-off value was 0.200, the diagnosis of regional LN metastasis in NSCLC sensitivity of 83.30% and specificity of 71.30% (AUC of 0.780 [95% CI, 0.720-0.830]). In our study, LN-SUVmax/PT-SUVmax was statistically different in the differential diagnosis of metastatic and non-metastatic LN ($P=0.039$), with a trend similar to previous studies. However, for FDG-avid LNs, although there is a high sensitivity, the specificity is still low. In our study, when we tried to use the dynamic metabolic parameter K_i/K_1 ratio for prediction, we found that the K_i/K_1 also has good diagnostic efficacy, especially for in the hilar region LNs.

The density, short and long diameters derived from CT images have been studied frequently in the differential diagnosis of benign and malignant lesions. Dwamena et al. (39) conducted a meta-analysis, which included 29 studies (2226 patients) from 1990 to 1998, to evaluate the accuracy of CT in lung cancer mediastinal staging, with a sensitivity of 0.60 (95% CI, 0.58-0.62), specificity of 0.77 (95% CI, 0.75-0.79), and accuracy of 0.75 (95% CI, 0.74-0.76). However, the results of our study showed

CT density, short diameter, and long diameter had no statistical difference (all $P>0.05$). Compared to CT imaging, the PET/CT improves the sensitivity and specificity of N-staging for lung cancer (40). However, both tumor and inflammatory lesions exhibit high FDG uptake (41, 42). Some lung cancer patients are often associated with underlying lung disease (e.g., tuberculosis, chronic obstructive pneumonia), especially in the elderly. Thus, in our study, the SUVmax had low specificity in FDG-avid LNs diagnosis, similar to the findings of previous studies (7, 8, 40).

Furthermore, previous studies have concluded that (24, 43, 44), SUVmax seemed to be more useful in predicting the benign and malignant LNs in the mediastinal area rather than the pulmonary hilar area. Lin et al. (43) also concluded that the total false positive rate could reach 70% when SUVmax predicted LNs status in the pulmonary hilar area, and most of the false positive cases were due to anthracosis, followed by reactive hyperplasia and hyalinized granuloma. In our study, by ROC curve analysis, K_i and K_i/K_1 had high differential diagnostic specificity both in the mediastinal region and pulmonary hilar region. Therefore, we believed that dynamic metabolic parameters, especially K_i , improved the accuracy of N-staging in the mediastinal and/or pulmonary hilar area, and provided a better complementary value than SUVmax.

Interestingly in our study, N-stages in nine patients were re-staged when dynamic metabolic parameters were considered. Eight patients had a reduction in N-stage from N3/N2 to N1/N0 (shown in Figure 4), two had a reduction from N3 to N0 and two had a reduction from N3 to N1. One patient had an elevated N stage from the previous N0 to N1. Based on SUVmax alone, the FDG-avid LNs were hard to differentiate in this patient. However, dynamic metabolic parameters, especially K_i , seemed promising for accurate N-staging of lung cancer.

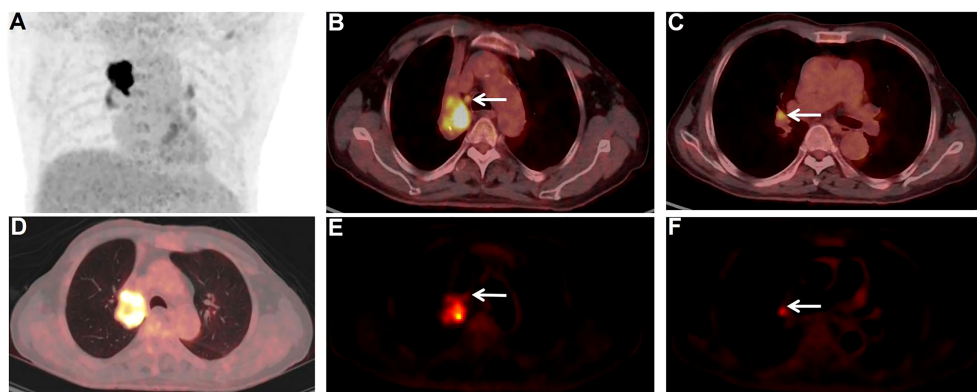


FIGURE 4

PET/CT images of non-metastatic and metastatic FDG-avid LNs. A 77-year-old male patient. Surgical pathology confirmed a squamous cell carcinoma in the upper lobe of the right lung. PET/CT scan showed multiple FDG-avid LNs in the mediastinal region and pulmonary hilar region. The FDG-avid LN (E, white arrow) in zone 4R (B, white arrow) of the mediastinal region was pathologically confirmed to be cancer-free, with a size of 0.7×0.6 cm, SUVmax of 4.0, and K_i of 0.0084 ml/g/min. The other FDG-avid LN (F, white arrow) in zone 11R (C, white arrow) of the pulmonary hilar region was pathologically proven to be metastases, with a size of 0.7×0.7 cm, SUVmax of 4.9, and K_i of 0.0202 ml/g/min.

Our study had several limitations. First, we excluded many patients without corresponding lesions in both PET/CT scans and puncture/surgery sites, thus this study was performed on relatively small sample size. Second, we collected fewer patients with benign lung lesions (tuberculosis, mechanized pneumonia), so we only studied FDG-avid LNs of lung cancer. Therefore, further study with expanded disease types and the sample size is needed to validate the current conclusion. Third, SUVmax rather than SUVmean was used in this study as we thought SUVmax was considered to be more stable and less affected by the partial volume effects (45–47). Fourth, motion correction was not considered in this study. It is known that motion in the chest region can affect not only the SUV but also the kinetic parameters quantification (48–51). Dedicated motion correction may be required to improve the accuracy of diagnosis in future studies.

Conclusions

In addition to SUVmax, dynamic metabolic parameters demonstrated good complementary values in improving the accuracy of N-staging in lung cancer. The K_1 , k_2 , K_i and K_i/K_1 showed promising potential for differential diagnosis of FDG-avid LNs in lung cancer. The K_i and K_i/K_1 had a high differential diagnostic value both in the mediastinal region and pulmonary hilar region.

Data availability statement

The original contributions presented in the study are included in the article/supplementary material. Further inquiries can be directed to the corresponding authors.

Ethics statement

This study was approved by the ethics committee of Cancer Hospital & Shenzhen Hospital, Chinese Academy of Medical Sciences (KYLH2022-1). The patients/participants provided their written informed consent to participate in this study.

References

1. Siegel RL, Miller KD, Fuchs HE, Jemal A. Cancer statistics, 2022. *CA: Cancer J Clin* (2022) 72(1):7–33. doi: 10.3322/caac.21708
2. Yang D, Liu Y, Bai C, Wang X, Powell CA. Epidemiology of lung cancer and lung cancer screening programs in China and the united states. *Cancer Lett* (2020) 468:82–87. doi: 10.1016/j.canlet.2019.10.009
3. Detterbeck FC, Postmus PE, Tanoue LT. The stage classification of lung cancer: Diagnosis and management of lung cancer, 3rd ed: American college of

Author contributions

XW and YL designed the project and write the manuscript. TS and ZW provided software, technical support and professional guidance. YZ analyzed data. ZZ, BH and SH organized data. YH and PW contribution FDG verification and injection. MZ and ML contribute to PET/CT scans. All authors contributed to the article and approved the submitted version.

Funding

This research was funded by National Cancer Center, National Clinical Research Center for Cancer, Cancer Hospital & Shenzhen Hospital, Chinese Academy of Medical Sciences and Peking Union Medical College, Shenzhen (SZ2020MS008), Shenzhen High-level Hospital Construction Fund, and Shenzhen Science and Technology Innovation Committee (JCYJ20220531100209020).

Conflict of interest

The authors declare that the research was conducted in the absence of any commercial or financial relationships that could be construed as a potential conflict of interest.

Publisher's note

All claims expressed in this article are solely those of the authors and do not necessarily represent those of their affiliated organizations, or those of the publisher, the editors and the reviewers. Any product that may be evaluated in this article, or claim that may be made by its manufacturer, is not guaranteed or endorsed by the publisher.

Supplementary material

The Supplementary Material for this article can be found online at: <https://www.frontiersin.org/articles/10.3389/fonc.2022.1005924/full#supplementary-material>

chest physicians evidence-based clinical practice guidelines. *Chest* (2013) 143(5 Suppl):e191S–210S. doi: 10.1378/chest.12-2354

4. Goldstraw P, Chansky K, Crowley J, Rami-Porta R, Asamura H, Eberhardt WE, et al. The IASLC lung cancer staging project: Proposals for revision of the TNM stage groupings in the forthcoming (Eighth) edition of the TNM classification for lung cancer. *J Thorac oncol: Off Publ Int Assoc Study Lung Cancer* (2016) 11(1):39–51. doi: 10.1016/j.jtho.2015.09.009

5. Woodard GA, Jones KD, Jablons DM. Lung cancer staging and prognosis. *Cancer Treat Res* (2016) 170:47–75. doi: 10.1007/978-3-319-40389-2_3
6. Ettinger DS, Wood DE, Aisne DL, Akerley W, Bauman JR, Bharat A, et al. NCCN guidelines insights: Non-small cell lung cancer, version 2.2021. *J Natl Compr Cancer Netw: JNCCN* (2021) 19(3):254–66. doi: 10.6004/jnccn.2021.0013
7. Zhao L, He Z-Y, Zhong X-N, Cui ML. (18) FDG-PET/CT for detection of mediastinal nodal metastasis in non-small cell lung cancer: a meta-analysis. *Surg Oncol* (2012) 21(3):230–6. doi: 10.1016/j.suronc.2011.11.001
8. Wu Y, Li P, Zhang H, Shi Y, Wu H, Zhang J, et al. Diagnostic value of fluorine 18 fluorodeoxyglucose positron emission tomography/computed tomography for the detection of metastases in non-small-cell lung cancer patients. *Int J Cancer* (2013) 132(2):E37–47. doi: 10.1002/ijc.27779
9. Schmidt-Hansen M, Baldwin DR, Zamora J. FDG-PET/CT imaging for mediastinal staging in patients with potentially resectable non-small cell lung cancer. *JAMA* (2015) 313(14):1465–6. doi: 10.1001/jama.2015.2365
10. Deppen S, Putnam JB, Andrade G, Speroff T, Nesbitt JC, Lambright ES, et al. Accuracy of FDG-PET to diagnose lung cancer in a region of endemic granulomatous disease. *Ann Thorac Surg* (2011) 92(2):428–32. doi: 10.1016/j.athoracsur.2011.02.052
11. Metser Ur, Even-Sapir E. Increased (18)F-fluorodeoxyglucose uptake in benign, nonphysiologic lesions found on whole-body positron emission tomography/computed tomography (PET/CT): accumulated data from four years of experience with PET/CT. *Semin Nucl Med* (2007) 37(3):206–22. doi: 10.1053/j.semnuclmed.2007.01.001
12. Deppen SA, Blume JD, Kensinger CD, Morgan AM, Aldrich MC, Massion PP, et al. Accuracy of FDG-PET to diagnose lung cancer in areas with infectious lung disease: a meta-analysis. *JAMA* (2014) 312(12):1227–36. doi: 10.1001/jama.2014.11488
13. Karakatsanis NA, Lodge MA, Tahari AK, Zhou Y, Wahl RL, Rahmim A. Dynamic whole-body PET parametric imaging: I. concept, acquisition protocol optimization and clinical application. *Phys Med Biol* (2013) 58(20):7391–418. doi: 10.1088/0031-9155/58/20/7391
14. Rahmim A, Lodge MA, Karakatsanis NA, Panin VY, Zhou Y, McMillan A, et al. Dynamic whole-body PET imaging: principles, potentials and applications. *Eur J Nucl Med Mol Imaging* (2019) 46(2):501–18. doi: 10.1007/s00259-018-4153-6
15. Gupta N, Gill H, Graeber G, Bishop H, Hurst J, Stephens T. Dynamic positron emission tomography with f-18 fluorodeoxyglucose imaging in differentiation of benign from malignant lung/mediastinal lesions. *Chest* (1998) 114(4):1105–11. doi: 10.1378/chest.114.4.1105
16. Meijer TWH, Geus-Oei L-Fde, Visser EP, Oyen WJG, Looijen-Salamon MG, Visvikis D, et al. Tumor delineation and quantitative assessment of glucose metabolic rate within histologic subtypes of non-small cell lung cancer by using dynamic 18F fluorodeoxyglucose PET. *Radiology* (2017) 283(2):547–59. doi: 10.1148/radiol.2016160329
17. Laffon E, Calcagni ML, Galli G, Giordano A, Capotosti A, Marthan R, et al. Comparison of three-parameter kinetic model analysis to standard patlak's analysis in 18F-FDG PET imaging of lung cancer patients. *EJNMMI Res* (2018) 8(1):24. doi: 10.1186/s13550-018-0369-5
18. Braune A, Hofheinz F, Bluth T, Kiss T, Wittenstein J, Scharffenberg M, et al. Comparison of static and dynamic 18F-FDG PET/CT for quantification of pulmonary inflammation in acute lung injury. *J Nucl medicine: Off publication Soc Nucl Med* (2019) 60(11):1629–34. doi: 10.2967/jnumed.119.226597
19. Coello C, Fisk M, Mohan D, Wilson FJ, Brown AP, Polkey MI, et al. Quantitative analysis of dynamic 18F-FDG PET/CT for measurement of lung inflammation. *EJNMMI Res* (2017) 7(1):47. doi: 10.1186/s13550-017-0291-2
20. Patlak CS, Blasberg RG, Fenstermacher JD. Graphical evaluation of blood-to-brain transfer constants from multiple-time uptake data. *J Cereb Blood Flow Metab: Off J Int Soc Cereb Blood Flow Metab* (1983) 3:1–7. doi: 10.1038/jcbfm.1983.1
21. Lawson CL, Hanson RJ. Solving least squares problems. *Linear Least Squares Linear Inequality Constraints* (1995) 23:158–73. doi: 10.1137/19781611971217:158-173
22. El-Sherief AH, Lau CT, Wu CC, Drake RL, Abbott GF, Rice TW. International association for the study of lung cancer (IASLC) lymph node map: radiologic review with CT illustration. *Radiographics: Rev Publ Radiol Soc North America Inc* (2014) 34(6):1680–91. doi: 10.1148/rg.346130097
23. Deterbeck FC, Boffa DJ, Kim AW, Tanoue LT. The eighth edition lung cancer stage classification. *Chest* (2017) 151(1):193–203. doi: 10.1016/j.chest.2016.10.010
24. Tournoy KG, Maddens S, Gosselin R, Van Maele G, van Meerbeek JP, Kelles A. Integrated FDG-PET/CT does not make invasive staging of the intrathoracic lymph nodes in non-small cell lung cancer redundant: a prospective study. *Thorax* (2007) 62(8):696–701. doi: 10.1136/thx.2006.072959
25. Kuo W-H, Wu Y-C, Wu C-Y, Ho KC, Chiu PH, Wang CW, et al. Node/aorta and node/liver SUV ratios from (18)F-FDG PET/CT may improve the detection of occult mediastinal lymph node metastases in patients with non-small cell lung carcinoma. *Acad Radiol* (2012) 19(6):685–92. doi: 10.1016/j.acra.2012.02.013
26. Schmidt-Hansen M, Baldwin DR, Hasler E, Zamora J, Abaira V, Roqué Figuls I M. PET-CT for assessing mediastinal lymph node involvement in patients with suspected resectable non-small cell lung cancer. *Cochrane Database Syst Rev* (2014) 13(11):CD009519. doi: 10.1002/14651858.CD009519.pub2
27. Yang DD, Mirvis E, Goldring J, Patel ARC, et al. Improving diagnostic performance of 18F-FDG-PET/CT for assessment of regional nodal involvement in non-small cell lung cancer. *Clin Radiol* (2019) 74(10):818.e17–818.e23. doi: 10.1016/j.crad.2019.07.009
28. Hellwig D, Graeter TP, Ukena D, Groeschel A, Sybrecht GW, Schaefer H-J, et al. 18F-FDG PET for mediastinal staging of lung cancer: which SUV threshold makes sense? *J Nucl medicine: Off publication Soc Nucl Med* (2007) 48(11):1761–6. doi: 10.2967/jnumed.107.044362
29. Dunnwald LK, Doot RK, Specht JM, Gralow JR, Ellis GK, Livingston RB, et al. PET tumor metabolism in locally advanced breast cancer patients undergoing neoadjuvant chemotherapy: value of static versus kinetic measures of fluorodeoxyglucose uptake. *Clin Cancer Res: An Off J Am Assoc Cancer Res* (2011) 17(8):2400–9. doi: 10.1158/1078-0432.CCR-10-2649
30. Nishimura M, Tamaki N, Matsushima S, Kiba M, Kotani T, Bamba C, et al. Dynamic whole-body 18F-FDG PET for differentiating abnormal lesions from physiological uptake. *Eur J Nucl Med Mol Imaging* (2020) 47(10):2293–300. doi: 10.1007/s00259-020-04726-w
31. Prost Nde, Feng Y, Wellman T, Tucci MR, Costa EL, Musch G, et al. 18F-FDG kinetics parameters depend on the mechanism of injury in early experimental acute respiratory distress syndrome. *J Nucl medicine: Off publication Soc Nucl Med* (2014) 55(11):1871–7. doi: 10.2967/jnumed.114.140962
32. Sachpekidis C, Hassel JC, Kopp-Schneider A, Haberkorn U, Dimitrakopoulou-Strauss A. Quantitative dynamic 18F-FDG PET/CT in survival prediction of metastatic melanoma under PD-1 inhibitors. *Cancers* (2021) 13(5):1019. doi: 10.3390/cancers13051019
33. Yang Z, Zan Y, Zheng X, Hai W, Chen K, Huang Q, et al. Dynamic FDG-PET imaging to differentiate malignancies from inflammation in subcutaneous and in situ mouse model for non-small cell lung carcinoma (NSCLC). *PLoS One* (2015) 10(9):e0139089. doi: 10.1371/journal.pone.0139089
34. Ye Q, Wu J, Lu Y, Naganawa M, Gallezot JD, Ma T, et al. Improved discrimination between benign and malignant LDCT screening-detected lung nodules with dynamic over static 18F-FDG PET as a function of injected dose. *Phys Med Biol* (2018) 63(17):175015. doi: 10.1088/1361-6560/aad97f
35. Yang M, Lin Z, Xu Z, Li D, Lv W, Yang S, et al. Influx rate constant of 18F-FDG increases in metastatic lymph nodes of non-small cell lung cancer patients. *Eur J Nucl Med Mol Imaging* (2020) 47(5):1198–208. doi: 10.1007/s00259-020-04682-5
36. Kajáry Kornélia, Lengyel Z, Tóké Anna-Mária, Kulka J, Dank M, Tóké T. Dynamic FDG-PET/CT in the initial staging of primary breast cancer: Clinicopathological correlations. *Pathol Oncol Res: POR* (2020) 26(2):997–1006. doi: 10.1007/s12253-019-00641-0
37. Cerfolio RJ, Bryant AS. Ratio of the maximum standardized uptake value on FDG-PET of the mediastinal (N2) lymph nodes to the primary tumor may be a universal predictor of nodal malignancy in patients with non-small-cell lung cancer. *Ann Thorac Surg* (2007) 83(5):1826–9. doi: 10.1016/j.athoracsur.2006.12.034
38. Fortuny MS, Gallego M, Berna LI, Montón C, Vigil L, Masdeu MJ, et al. FDG-PET parameters predicting mediastinal malignancy in lung cancer. *BMC Pulm Med* (2016) 16(1):177. doi: 10.1186/s12890-016-0338-6
39. Dwamena BA, Sonnad SS, Angobaldo JO, Wahl RL. Metastases from non-small cell lung cancer: mediastinal staging in the 1990s—meta-analytic comparison of PET and CT. *Radiology* (1999) 213(2):530–6. doi: 10.1148/radiology.213.2.r99nv4653
40. Wu L-M, Xu J-R, Gu H-Y, Hua J, Chen J, Zhang W, et al. Preoperative mediastinal and hilar nodal staging with diffusion-weighted magnetic resonance imaging and fluorodeoxyglucose positron emission tomography/computed tomography in patients with non-small-cell lung cancer: which is better? *J Surg Res* (2012) 178(1):304–14. doi: 10.1016/j.jss.2012.03.074
41. Pijl JP, Nienhuis PH, Kwee TC, Glaudemans AWJM, Slart RHJA, Gormsen LC. Limitations and pitfalls of FDG-PET/CT in infection and inflammation. *Semin Nucl Med* (2021) 51(6):633–45. doi: 10.1053/j.semnuclmed.2021.06.008
42. Love C, Tomas MB, Tronco GG, Palestro CJ. FDG PET of infection and inflammation. *Radiographics: Rev Publ Radiol Soc North America Inc* (2005) 25(5):1357–68. doi: 10.1148/rg.255045122
43. Lin W-Y, Hsu W-H, Lin K-H, Wang SJ. Role of preoperative PET-CT in assessing mediastinal and hilar lymph node status in early stage lung cancer. *J Chin Med Assoc: JCMA* (2012) 75(5):203–8. doi: 10.1016/j.jcma.2012.04.004
44. Billé A, Pelosi E, Skanjeti A, Arena V, Errico L, Borasio P, et al. Preoperative intrathoracic lymph node staging in patients with non-small-cell lung cancer:

accuracy of integrated positron emission tomography and computed tomography. *Eur J cardio-thoracic surgery: Off J Eur Assoc Cardio-thoracic Surg* (2009) 36 (3):440–5. doi: 10.1016/j.ejcts.2009.04.003

45. Hoffman EJ, Huang SC, Phelps ME. Quantitation in positron emission computed tomography: 1. effect of object size. *Journal of Computer Assisted Tomography* (1979) 3(3):299–308. doi: 10.1097/00004728-197906000-00001

46. Rousset OG, Ma Y, Evans AC. Correction for partial volume effects in PET: principle and validation. *J Nucl medicine: Off publication Soc Nucl Med* (1998) 39 (5):904–11.

47. Chang G, Chang T, Pan T, Clark JW Jr, Mawlawi OR. Joint correction of respiratory motion artifact and partial volume effect in lung/thoracic PET/CT imaging. *Med Phys* (2010) 37(12):6221–32. doi: 10.1118/1.3512780

48. Sarikaya I, Yeung HWD, Erdi Y, Larson SM. Respiratory artefact causing malpositioning of liver dome lesion in right lower lung. *Clin Nucl Med* (2003) 28 (11):943–4. doi: 10.1097/01.rlu.0000093095.28642.2b

49. Nehmeh SA, Erdi YE, Ling CC, Rosenzweig KE, Schoder H, Larson SM, et al. Effect of respiratory gating on quantifying PET images of lung cancer. *J Nucl medicine: Off publication Soc Nucl Med* (2002) 43(7):876–81.

50. Sun T, Petibon Y, Han PK, Ma C, Kim SJW, Alpert NM, et al. Body motion detection and correction in cardiac PET: Phantom and human studies. *Med Phys* (2019) 46(11):4898–906. doi: 10.1002/mp.13815

51. Sun T, Wu T-H, Wang S-J, Yang BH, Wu NY, Mok GS. Low dose interpolated average CT for thoracic PET/CT attenuation correction using an active breathing controller. *Med Phys* (2013) 40(10):102507. doi: 10.1118/1.4820976